17th World Conference on Earthquake Engineering, 17WCEE
Sendai, Japan - September 13th to 18th 2020

NUMERICAL MODELLING OF THE PLASTIC HINGE OF GIRDERS IN STEEL MOMENT RESISTING FRAMES

R. Herrera[(1)], N. Leiva[(2)], L. Massone[(3)], J. Beltran[(4)]

[(1)] *Associate professor, Department of Civil Engineering, University of Chile, riherrer@ing.uchile.cl*
[(2)] *Research Assistant, Department of Civil Engineering, University of Chile, nleivaf@gmail.com*
[(3)] *Associate professor, Department of Civil Engineering, University of Chile, lmassone@uchile.cl*
[(4)] *Associate professor, Department of Civil Engineering, University of Chile, jbeltran@ing.uchile.cl*

...

Abstract

One of the energy dissipation mechanisms in moment resisting frames is the formation of plastic hinges on girders. The inelastic rotation capacity of these hinges is limited by the degree of strength deterioration once the maximum moment has been reached. This characteristic is highly influenced by the onset of local buckling in the plastic hinge region, once a significant portion of the cross section has reached the yield stress. The response of plastic hinges on steel girders has been the subject of numerous studies, but so far only models based on calibration against experimental results or based on an average response are available. This work presents a numerical model of the plastic hinge region on a girder based on an assumed plastic hinge length and a geometrical imperfection corresponding to the fabrication tolerance established in a widely used steel standard. The model consists on a series of uniaxial bars that work under tension and compression, spanning the plastic hinge length, each one corresponding to a fiber of the cross section. The Euler-Bernoulli hypothesis is imposed on the ends of the plastic hinge region and elastic bars are used to model the girder outside this region. The model was validated against experimental results from three different connection tests subjected to cyclic loading. From the comparison of experimental and numerical results, it is observed that the model is capable of representing the response of the plastic hinge properly, both in terms of strength and strength degradation, requiring only the information of the material properties, the geometry of the specimen, the expected plastic hinge length, and the standard fabrication tolerances.

Keywords: plastic hinge; numerical model; steel; moment resisting frame; cyclic loading

1. Introduction

Structural steel is a construction material known for having the highest strength to weight ratio and significant ductility. These characteristics have made its use particularly appealing for earthquake resistant structures. When the flexural response of a steel member in a structure is the controlling factor for the strength and deformation capacity of the structure (e.g. moment resisting frames), the optimum mechanism of energy dissipation is the formation of flexural plastic hinges in the member. From a design standpoint, the ability to form plastic hinges with a significant inelastic deformation capacity is controlled by limiting the slenderness of the elements that form the cross section. However, when the objective is to determine the performance of a member or a structural system under earthquake loading conditions, a more refined model for the plastic hinge is required. The model must be able to reproduce not only the strength, but also the ductility and strength degradation of the plastic hinge.

The purpose of this work is to numerically reproduce, using a finite length plastic hinge, the response of a steel beam subjected to bending, that induces the formation of plastic hinges near the ends of the connection region. The novelty of the modeling scheme proposed is that it requires fewer assumptions than previous models based on line elements, and it is computationally less expensive than full 3D finite element models.

2. Previous research

The model presented in this paper is an extension of the work of Massone and Moroder [1]. These authors developed a numerical model to simulate the buckling of a reinforcing bar, located on the edge of a reinforced concrete element subjected to compression, bending and shear forces. The model, shown in Fig. 1, has one end fixed and the other restrained to rotate and move out of plane, but free to move in the axial direction. The bar contains an initial imperfection e, that induces the lateral displacement w in the middle. The buckling of the bar is represented as this lateral displacement w, and also through an angle θ_p that is function of the displacement w. The forces on the reinforced concrete element are transferred to the reinforcing bar as compression and tension, generating increasing out-of-plane displacement of the bar, which after certain level of axial displacement induces the formation of plastic hinges, followed by the loss of strength associated with buckling of the bar. The compressive or buckling response depends on the ratio between the stirrup spacing and the bar diameter The authors found that the most adequate value for this ratio was about 8. Equilibrium is imposed in the deformed shape of the bar and sectional analysis is performed for the plastic hinge, where each fiber defined in the section is based on the steel material formulation developed by Chang and Mander [2].

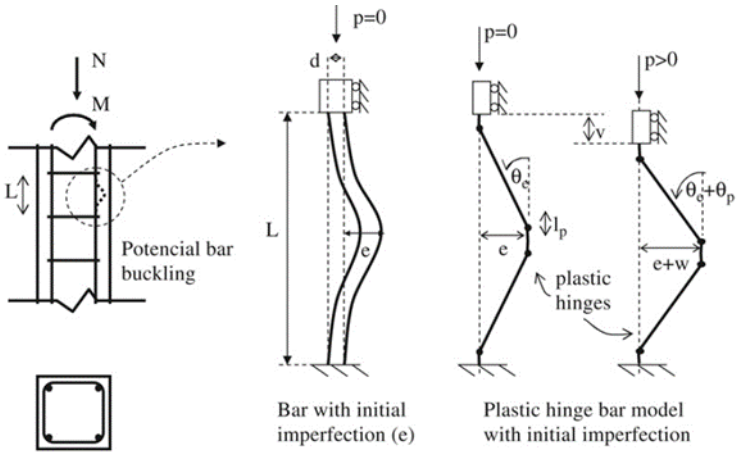

Fig. 1 – Schematic of reinforcing bar buckling model with initial imperfection (Massone & Moroder [1]).

In order to validate the model, steel connection tests results were obtained from two sources: 1) SAC Steel Project [3], financed by the Federal Emergency Management Agency (FEMA), and 2) the test conducted at ATLSS Research Center, Lehigh University, by Ricles et al [4]. Three tests were selected: one exterior connection (Test #1) and two interior connections (Tests #2 and #3). The main characteristics of every test are listed on Table 1 and a schematic of each configuration in Fig. 2. The displacement history applied to the specimens is presented in Fig. 3. Fig. 4 shows the state of the specimens at the end of the test for Test#1 and Test#2. The formation of the plastic hinges on the beams is apparent.

Table 1 – Characteristics of tests used for validation

	Column Section	Beam Section	Grade	Connection	Lateral Restriction
Test #1	W 14x176	W 30x99	A572, Gr. 50	Welded flange plate	No
Test #2	W 14x398	W36x150	A572, Gr. 50	WUF, pre-Northridge	Yes
Test #3	CFT 16x16x1/2	W 24x62	----	Double Split T	Yes

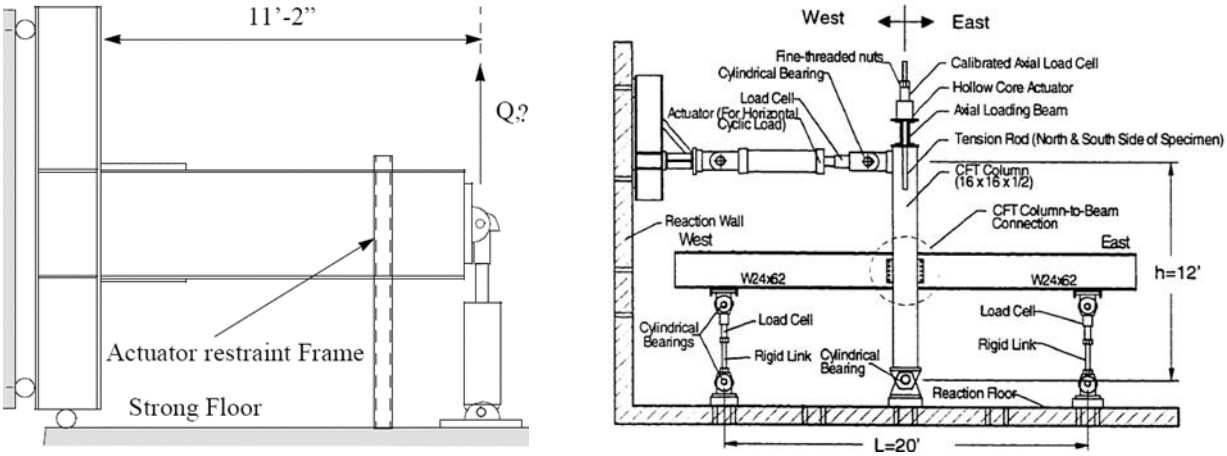

(a) Exterior connection [3] (b) Interior connection [4]

Fig. 2 – Configurations of tests used for validation

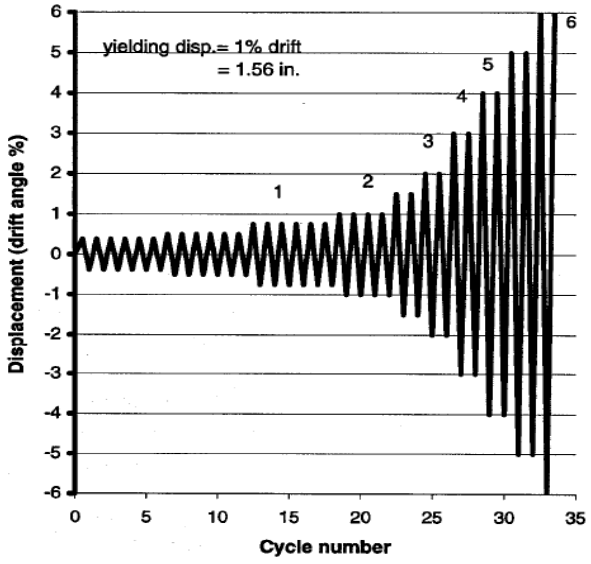

Fig. 3 – Displacement history applied to the specimens [3]

(a) Test #1 (b) Test #2

Fig. 4 – Specimens after testing [3]

3. Numerical model

The model is a planar model composed of one or two beams, a connection region, a panel zone, and an elastic column. The model is constructed and analyzed using Opensees [5]. In the case of the exterior column model, shown in Fig. 5, the beam has one free end where the load is applied and the column is simply supported.

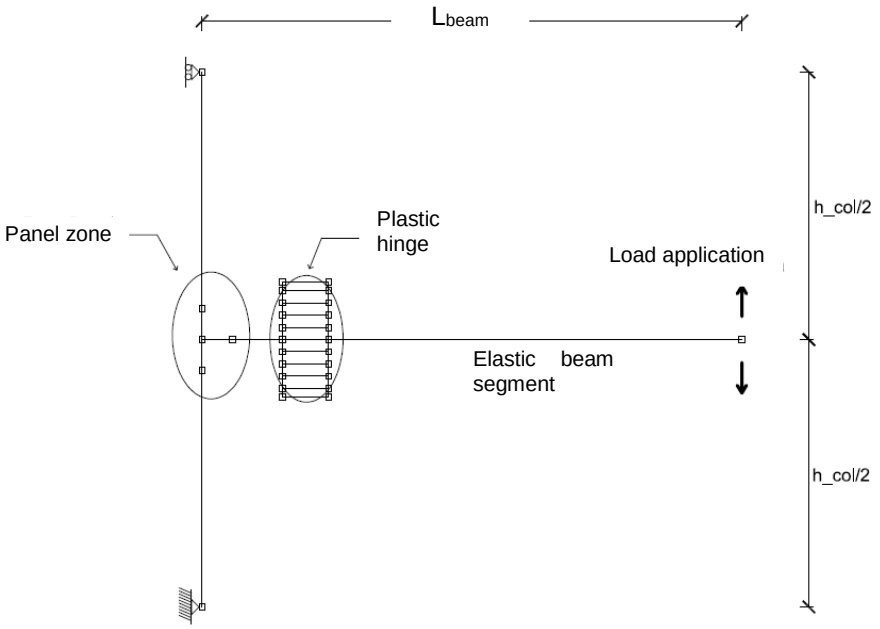

Fig. 5 – Outline of exterior column model.

For the case of the interior column model, shown in Fig,6, the beams have roller supports on the ends, and the column is simply supported at the base, but free at the top, where the load is applied.

The analysis is displacement controlled at the node where the load is applied, following the test displacement history shown in Fig. 3.

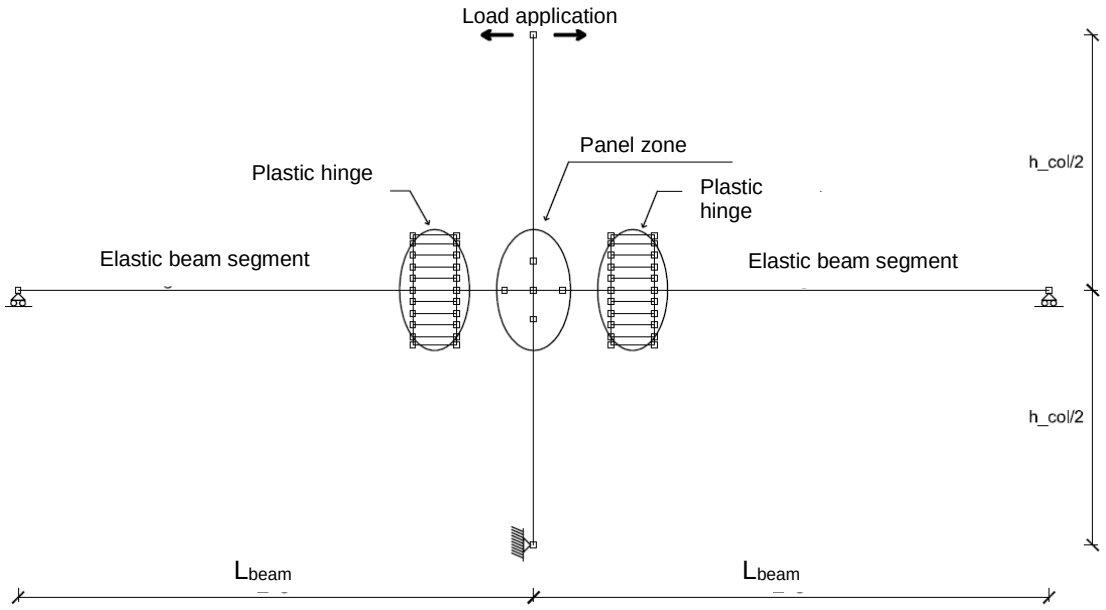

Fig. 6 – Scheme of interior column model.

3.1. Beam model

The beam-connection model is divided in 4 zones with different material and level of detail, depending on the expected behaviour and the computational cost associated. The 4 zones, shown in Fig.7, are: 1) linear elastic beam zone; 2) plastic hinge zone; 3) connection zone, 4) rigid zone. Zone 1 connects end away from the column with the plastic hinge, and has identical properties to the beam used in the test. Zone 2 is the plastic hinge zone, which is the contribution of this work and will be detailed later. Zone 3 is also linear elastic with sectional properties of the beam plus any reinforcement existing in the connection area. Welds and shear plates are not considered in the model. Finally, Zone 4 is a rigid element of length equal to half the depth of the column that represents the region between the column face and the centerline of the column, part of the panel zone which will be discussed later too.

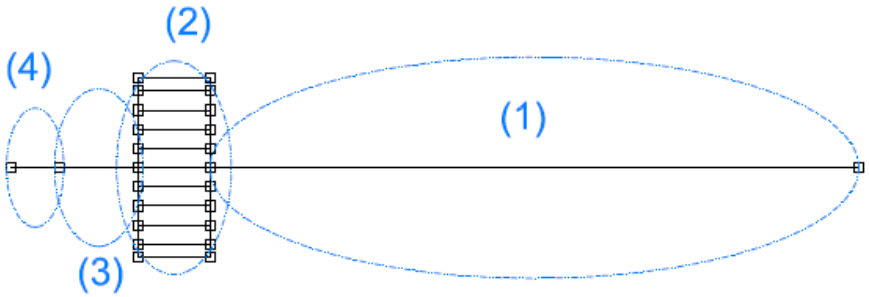

Fig. 7 – Scheme of beam-column model, divided in zones.

The elastic zones 1, 3 and 4 use the same type of element that corresponds to a force-based element. The section properties, area and moment of inertia, mimic the properties on the test. The elastic modulus used for the steel is 200.000 MPa. The connection between Zones 3 and 4 is considered fully rigid.

3.2. Column model

Elastic force based elements are also used for the columns. The cross section area and moment of inertia reproduce the test column sizes.

3.3. Panel zone

The model is composed exclusively of line elements, which for the beam and the column are located on the centerline of the member. The panel zone is considered rigid for this work, therefore rigid elements are used to join the node at the center of the panel zone with the nodes at the column face and at the locations of the beam flanges.

3.4. Plastic hinge model

The plastic hinge model considers material and geometric non linearities. It is a finite length plastic hinge model that represent the plastic hinge zone discretizing the beam in a number of round bars of length equal to the plastic hinge length, modeled using the bar model of Massone and Moroder [1]. Each bar is composed of 5 elements, as shown in Fig. 8. Each element is composed of an elastic part (thin black line in Fig. 8) and a nonlinear part (red line in Fig. 8). The elastic part is completely defined with only 3 parameters: elastic modulus E = 200000 MPa, area equal to area of the round section, and moment of inertia of the round section. The nonlinear part corresponds to a fiber section and the material is the one proposed by Chang and Mander [2].

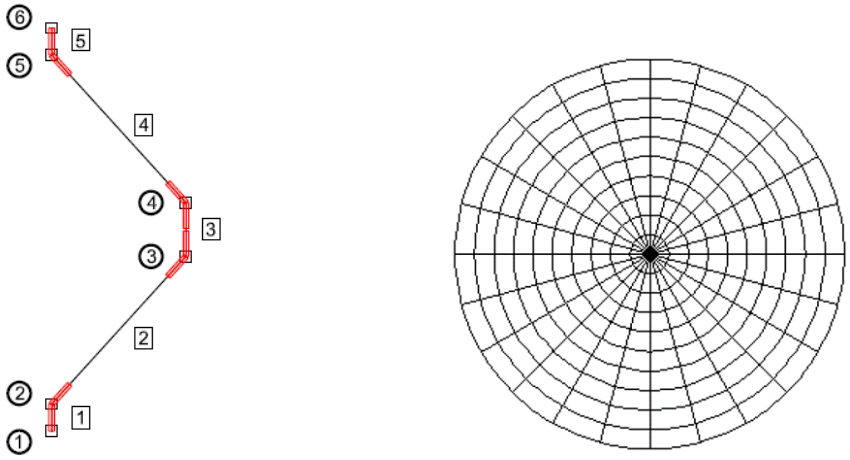

(a) Bar model (b) Bar fiber discretization

Fig. 8 – Scheme of bar model, nodes and elements named schematically.

Each bar is given an initial imperfection which varies linearly from zero at the intersection of web and flange to the maximum flange-tilt tolerance (def_{maxf}) of the AISC Code of Standard Practice [6] for wide flange beams, at the flange tips. The initial imperfection of the other flange bars is calculated using Eq. (1).

$$\left|def_{fj}\right| = \frac{def_{\max f} \cdot j}{n_f} \tag{1}$$

where j = 1, 2,…, n_f. The initial imperfection of the web bars varies from zero at the intersection of web and flanges to a maximum value (def_{maxw}) at the center of the web. The initial imperfection for the other web bars is calculated using Eq. (2).

$$\left|def_{wi}\right| = \frac{def_{\max w} \cdot (n_w - i + 1)}{(n_w + 1)} \tag{2}$$

The initial imperfection values are expressed as an absolute value. For the purpose of the model it is not relevant whether the imperfection is modeled upwards or downwards.

The bars are spatially distributed according to the cross section, as illustrated in Fig. 9. The flanges are divided in an even number of bars ($2n_f$), while the web is discretized using an odd number of bars ($2n_w$+1), in order to ensure that there will always be one bar at the center of the web. Each circular bar section

corresponds to a rectangular segment of the flange or the web. Hence, in general, web and flange bars have different diameters ϕ_f and ϕ_w, respectively. These values are calculated by equating the area of the rectangular piece of beam flange or beam web with the area of the corresponding round flange or web bar, respectively, as shown by Eq. (3) and Eq. (4).

$$\phi_f = \sqrt{\frac{2t_{fb} \cdot b_b}{\pi \cdot n_f}} \tag{3}$$

$$\phi_w = \sqrt{\frac{4t_{wb} \cdot (h_b - 2t_{fb})}{\pi \cdot (2n_w + 1)}} \tag{4}$$

where b_b and t_{fb} are the flange width and flange thickness, respectively, and h_b and t_{wb} correspond to the web height and web thickness.

The number of bars used on the web and flanges is controlled by the ratio l/ϕ, where l is the bar length (the plastic hinge length in this case) and ϕ is the bar diameter. This ratio has an upper bound, according to Massone and Moroder [1], above which the results are no longer reliable. Hence n_w and n_f depend on the size of the beam and the plastic hinge length assumed. For Tests #1 and #3, n_w = 4 was used, while for Test #2, n_w = 3. In the case of the flanges n_f = 2 is adequate for all tests. The length of the plastic hinge, L_{ph}, assumed was based on Haaijer [7] and Lay's [8] proposal, given by Eq. (5).

$$L_{ph} = 0.6\left(\frac{t_f}{t_w}\right)^{3/4}\left(\frac{2h}{b_f}\right)^{1/4} b_f \tag{5}$$

where b_f and t_f are the flange width and flange thickness, respectively, and h and t_w correspond to the web height and web thickness.

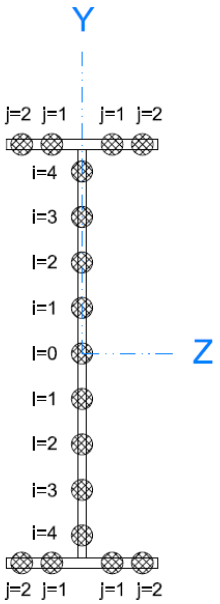

Fig. 9 – Spatial distribution of bars in flanges and web in wide flange beam section.

Euler-Bernoulli's hypothesis is assumed on the ends of the plastic hinge. To enforce it, rigid elements are used to maintain the plane section at these ends throughout the analysis. The nodes on the rigid bars are connected to the end nodes of the plastic hinge bars such that they have equal horizontal and vertical

displacements, but the rotations are independent. The rotations on the ends of the plastic hinge bars are restrained, to match the boundary conditions used by Massone and Moroder [1]. Fig. 10 shows the degrees of freedom (dof) of the nodes at the plastic hinge bar end (in black), and the dof of the nodes at both rigid plates (in blue). The restrained dof are crossed-out.

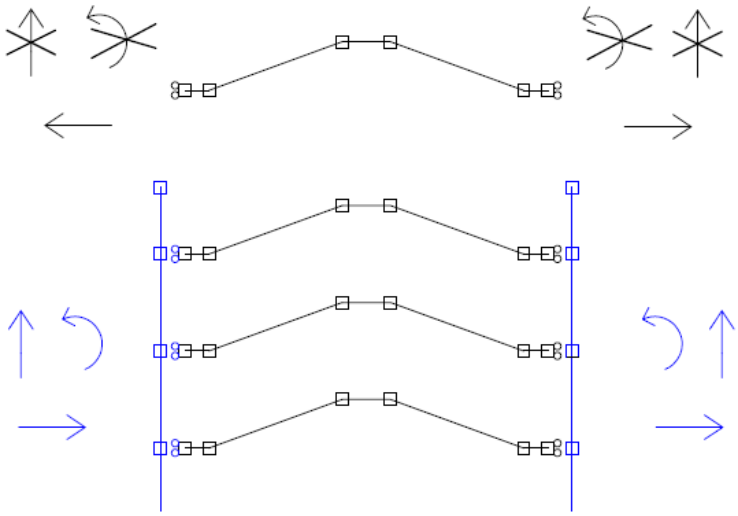

Fig. 10 – Degrees of freedom in the rigid end plates (in blue) and bar ends (in black)

3.5. General model details

The coordinate transformation chosen is "Corotational Transformation", that allows to solve problems with non-linear geometry. This coordinate transformation fixes the local coordinates to an element and moves simultaneously with it, displacing and turning at the same time, following the movement of the rigid body. Therefore, the stiffness matrices are formulated in this local system based on small deformations. Later on, they are transformed to the global coordinate system and assembled. Because this new geometry is unknown, an iterative approach must be used to equilibrate the structure resistant forces with the external forces of the new geometry. The integration method used is Gauss-Lobatto with 6 points quadrature, as recommended by Neuenhofer and Filippou [9].

4. Results and Analysis

The nominal displacement history applied during each test was imposed to every model at the corresponding point depending on its configuration. These displacements generate maximum bending moments at the beam-column joint and they activate the plastic hinge mechanism on the beam, generating tensile-compression cycles on the plastic hinge bars.

4.1. Comparison of model with experimental data

To validate the modelling assumptions, the numerical results are compared with experimental results for each of the three tests selected previously. The comparison is made in terms of either: 1) applied force versus displacement; or 2) plastic hinge moment versus plastic rotation.

4.1.1. Test #1

This test has the exterior column configuration, where the beam is a W30x99 and the column is a W14x176. The comparison of numerical and experimental results for applied force vs. displacement and plastic hinge moment vs. plastic rotation are shown in Fig. 11. The results are shown in imperial units because the original tests were reported using the imperial numerical system.

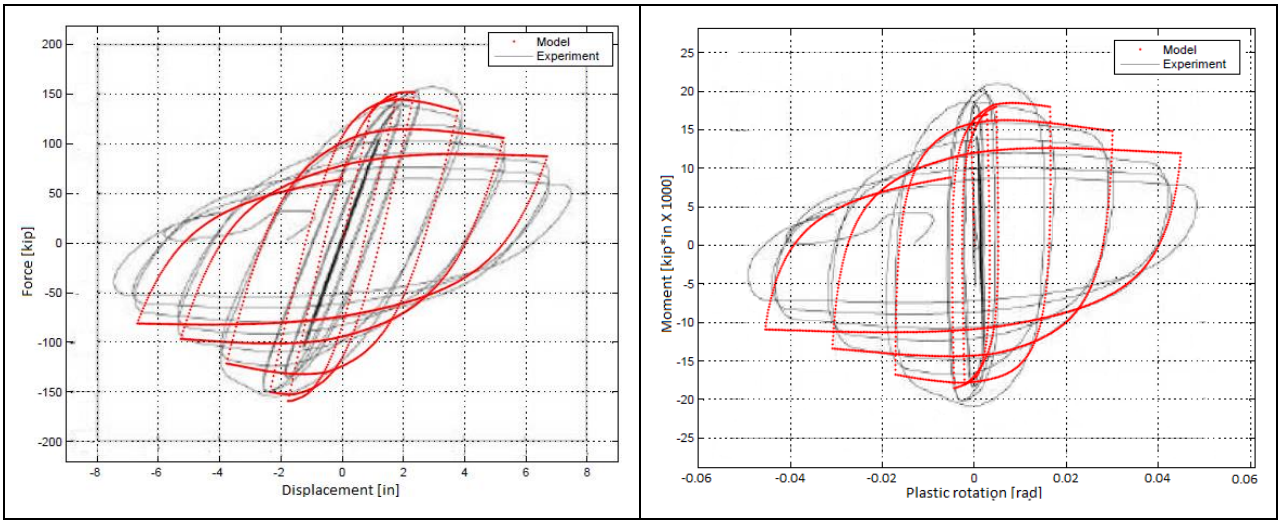

a) Force-displacement b) Moment-plastic rotation

Fig. 11 – Comparison between numerical model and experimental results for Test #1

Adequate agreement is observed between both curves, in terms of maximum resistance and degradation capacity in every cycle. The maximum model resistance has a difference of 5% with the Test#1. The numerical model results show symmetry in both directions of load application. Although the numerical model maximum moment in the first two cycles is smaller than the experimental maximum, this difference tends to disappear when the displacement increases.

4.1.2. Test#2

This test has an interior column configuration, and the tested beams are W36x150, while the column is a W14x398. The comparison of force and displacement between the numerical model and experimental results is shown in Fig. 12.

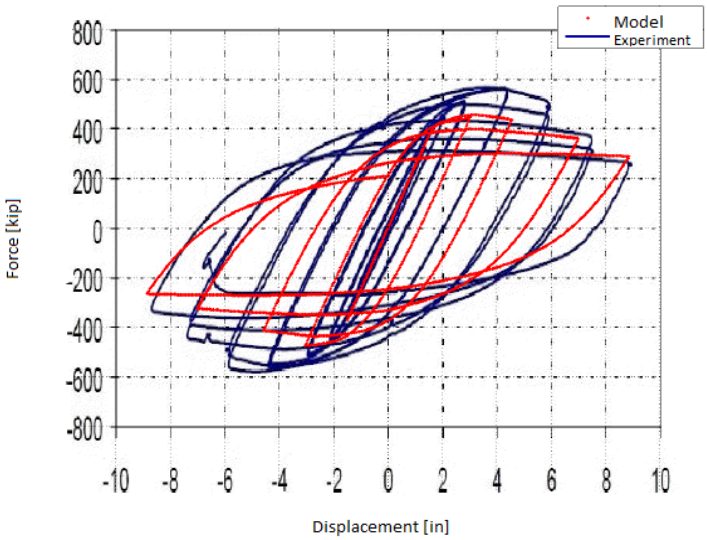

Fig. 12 – Force-displacement comparison between numerical model and experimental results. Test#2.

For this specimen, there is a more significant difference in strength (20% difference between model and experimental results), which tends to decrease as the capacity degrades for increasing displacements. It can also be observed that, for the first cycles, the stiffness of the numerical model compares favorably with the experimental stiffness. From parametric analyses conducted, which are not shown here due to space constrains, it is possible to improve the agreement between tests and numerical model by modifying the

plastic hinge length or changing the distribution of the plastic hinge bars. These results are not shown to maintain consistency in the assumptions for the three specimens.

Fig. 13 shows the comparison of bending moment vs plastic rotation between the numerical model and the experiments, for both beams. Although there is still a difference in capacity, the agreement is better than for the global response. The difference of maximum moment in this case diminish with incremental load cycles, disappearing for the largest cycles in the positive side, for the East beam. The experimental results show again a lack of symmetry between the positive and negative side. In the case of the West beam a significant lack of symmetry is observed in the experimental data, in contrast with model's symmetry. The model response shown in Fig. 13b) is identical to the observed in Fig. 13a), because it is the same plastic hinge model in the West and East beams, indicating that the differences in the experimental response between both beams is related to particular experimental unattended conditions.

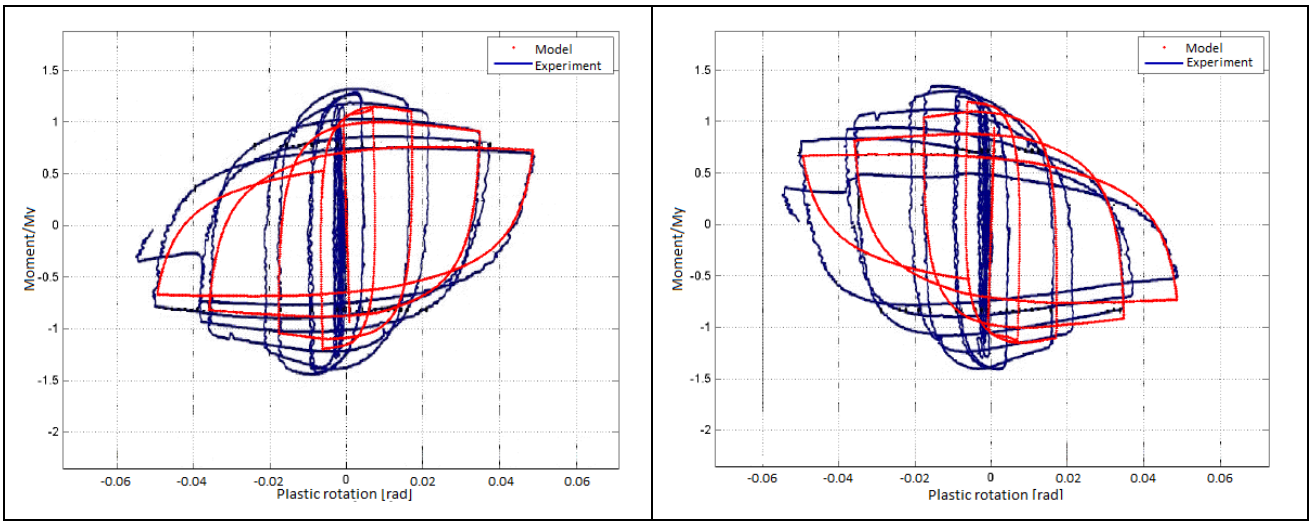

a) East beam b) West beam

Fig. 13 – Moment-plastic rotation comparison between numerical model and experimental results. Test#2.

4.1.3. Test#3

This test corresponds to an interior column configuration, where the test beams are W24x62 and the column is a concrete filled tube (CFT) 16x16x1/2. Model and experimental data are compared only for the bending moment - plastic rotation response in the plastic hinge zone. The comparison is shown in Fig. 14.

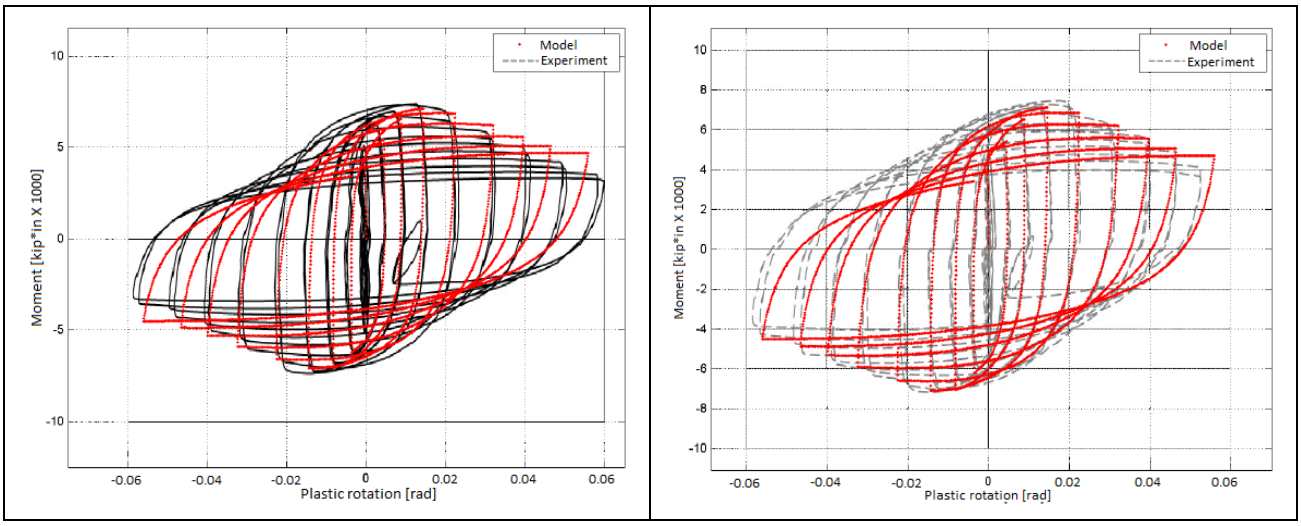

a) East beam b) West beam

Fig. 14 – Moment-plastic rotation comparison between model and experiments. Test#3.

Adequate agreement between the numerical model and the experimental results can be observed, particularly in terms of maximum strength.

5. Conclusions

The objective of the work presented here was to propose and validate a modelling strategy for beams subjected to bending moments that caused the formation of plastic hinges on the beam ends. Such behavior has been modeled in OpenSees [5] using uniaxial elements. The model considers a plastic hinge zone inserted in a beam-column configuration that has a lineal-elastic behavior.

The plastic hinge zone is constituted by a system of bars susceptible to buckling under tension-compression cycles. These bars consider an initial imperfection and a non-linear constitutive law to capture buckling and strength degradation. Through the use of rigid plates on both sides of the plastic hinge, the bars work as a unique system transforming the beam bending moment in tensile and compression of uniaxial elements.

The profile section works following the Bernoulli hypothesis, therefore the farthest bars deform more inelastically and degrade more its resistant capacity. The resistance of every bar depends on the relation l/ϕ and on the material properties. Moreover, the entire model is very sensitive to changes on the plastic hinge length and to the variation on the number of bars that compound the web and flanges.

From the results, it is observed that the model adequately represents the structural response of the tests. The differences observed for Test #2 are attributable to the relation l/ϕ, because its modification generates changes in the maximum resistance. However, major changes are observed in the degradation of resistance capacity.

In addition to the uncertainty of the model, the experimental uncertainty must be considered. Test #1 differs from the other two tests, because there was no lateral restraint for the beam. The incorporation of this failure mode may produce a reduction of the maximum resistant force and a diminution of the stiffness. The maximum model resistance has a difference of 5% with the Test#1, while the Test#2 differs on 20% with model results.

The precise representation of local buckling in the model is limited by the relation l/ϕ of the plastic hinge constitutive bars. However, this value does not vary continuously because it depends on the number of bars, which is a discrete value. The importance of this value makes desirable a model improvement that allows vary the l/ϕ value and then calibrate it to represent the beam local buckling in a better way.

Likewise, it is desirable to study the plastic hinge length estimation. The adopted expression may be subjected to errors, and has been chosen as a first approximation. It has been noticed that the plastic hinge length considerably affects the structural response of the model, and constitute a potential source of error. Another imprecision corresponds to the beam-column connection that might be improved to represent the column-beam interaction in a better way.

6. References

[1] Massone L, Moroder D (2008): Buckling modeling of reinforcing bars with imperfections. *Engineering Structures*, **31**(8), 758-767.

[2] Chang GA, Mander JB (1994): Seismic energy based fatigue damage analysis of bridge columns: Part I – Evaluation of Seismic capacity. *Technical Report NCEER-94-0006*, National Center for Earthquake Engineering Research, Buffalo, NY, USA.

[3] SAC Steel Project [on line] http://www.sacsteel.org [last consulted: June 2014].

[4] Ricles JM, Peng SW, Lu LW (2004): Seismic Behavior of Composite Concrete Filled Steel Tube Column-Wide

[5] OpenSees [on line] http://opensees.berkeley.edu [last consulted: August 2014].

[6] AISC (2016): ANSI/AISC 303-16. Code of Standard Practice for Steel Buildings and Bridges. *American Institute of Steel Construction*, Chicago, IL, USA

[7] Haaijer G (1957): Plate buckling in the strain-hardening range. *Journal of the Engineering Mechanics Division*, **83**(2), 1-47.

[8] Lay MG (1965): Flange local buckling in wide-flange shapes. *Journal of the Structural Division, ASCE*, **ST6**, 95-115.

[9] Neuenhofer A, Filippou F (1997): Evaluation of nonlinear frame finite-element models. *Journal of Structural Engineering*, **123**(7), 958-966.

